

Spontaneous vortex formation on a superconductor film

M. Donaire,¹ T.W.B. Kibble,² and A. Rajantie¹

¹*DAMTP, CMS, University of Cambridge, Wilberforce Road,
Cambridge CB3 0WA, United Kingdom*

²*Blackett Laboratory, Imperial College London,
London SW7 2AZ, United Kingdom*

(Dated: September 7, 2004)

We carry out numerical simulations to investigate spontaneous vortex formation during a temperature quench of a superconductor film from the normal to the superconducting phase in the absence of an external magnetic field. Our results agree roughly with quantitative predictions of the flux trapping scenario: In fast quenches the agreement is almost perfect, but there appears to be some discrepancy in slower ones. In particular, our simulations demonstrate the crucial role the electromagnetic field plays in this phenomenon, making it very different from vortex formation in superfluids. Besides superconductor experiments, our findings also shed more light on the possible formation of cosmic defects in the early universe.

I. INTRODUCTION

When a superconductor is rapidly cooled from the normal to the superconducting phase in the absence of an external magnetic field, vortices (and antivortices) form. This phenomenon has been observed in several experiments^{1,2,3,4,5,6,7,8} and has analogues in other condensed matter systems such as superfluids^{9,10,11} and liquid crystals.^{12,13,14,15} In the latter cases, the order parameter is electrically neutral and defect formation can be understood in terms of the Kibble-Zurek mechanism.^{16,17,18} In contrast, the Cooper pairs in superconductors are electrically charged, which means that the electromagnetic field plays an important role.^{19,20}

Understanding the mechanisms in which vortices form would also have implications well beyond condensed matter physics. In particular, similar mechanisms may have produced topological defects such as cosmic strings, magnetic monopoles and domain walls in the early universe,^{16,21} either in cosmological phase transitions¹⁷ or in brane collisions.²² This is particularly interesting, because two possible gravitational lensing events by cosmic strings have recently been observed.^{23,24,25}

In cosmology, a neutral order parameter corresponds to a global symmetry and a charged order parameter to a local gauge symmetry. In the latter case, which is more common, the vortices are Nielsen-Olesen cosmic strings.²⁶ The role of the Cooper pairs is played by the Higgs field, which obtains a non-zero vacuum expectation value at the transition.

In this paper, we investigate vortex formation in the case of a two-dimensional film in three-dimensional space. This is the relevant setup for actual superconductor experiments, but to our knowledge no simulations have been carried out in the past. While in the case of a neutral order parameter, a two-dimensional film can be studied using a fully two-dimensional simulation, the three-dimensional nature of the electromagnetic field means that the same is not true for superconductors.²⁷

Because our setup captures some of the peculiarities

of fully three-dimensional systems, it is also more relevant for cosmological applications than previous two-dimensional studies.²⁸ A different borderline case between two and three spatial dimensions has been studied in the past in Refs. 19 and 29.

II. SETUP

The system we shall study consists of a two-dimensional superconductor film in a three-dimensional space. The superconductor is described by the Ginzburg-Landau theory with an electrically charged order parameter that is confined to the film. In contrast, the electromagnetic field lives in the full three-dimensional space. We shall denote three-vectors by bold-faced letters (such as \mathbf{x}) and two-vectors on the film by letters with arrows on top (\vec{x}).

We consider a hypothetical experiment in which the whole system is first heated up to a temperature above T_c , so that the film is in the normal phase. Then the system is gradually cooled through the phase transition to the superconducting phase.

As usual, the two-dimensional Ginzburg-Landau (free) energy is written as

$$E_\psi = \int d^2x \left[\alpha |\psi|^2 + \frac{\beta}{2} |\psi|^4 + \frac{1}{2m} \left| (-i\hbar\vec{\nabla} - e\vec{A}) \psi \right|^2 \right]. \quad (1)$$

The field $\psi(x, y)$ is a complex scalar field, and the two-dimensional vector potential $\vec{A}(x, y)$ is obtained from the full three-dimensional $\mathbf{A}(x, y, z)$ by restricting to the plane $z = 0$, and x and y directions,

$$\vec{A}_x(x, y) = \mathbf{A}_x(x, y, 0), \quad \vec{A}_y(x, y) = \mathbf{A}_y(x, y, 0). \quad (2)$$

The energy of a three-dimensional electromagnetic field configuration is given by

$$E_{\mathbf{A}} = \int d^3x \left[\frac{\epsilon_0 \mathbf{E}^2}{2} + \frac{\mathbf{B}^2}{2\mu_0} \right], \quad (3)$$

where $\mathbf{B} = \nabla \times \mathbf{A}$ is the magnetic field (or induction) and \mathbf{E} is the electric field. If we choose the temporal gauge, we can write $\mathbf{E} = -\partial\mathbf{A}/\partial t$. In what follows, we shall simplify the notation by choosing a unit system in which $m = 1/2$, $c = \hbar = \mu_0 = \epsilon_0 = k_B = 1$.

Because we are interested in the time evolution of the system, we need to include the kinetic energy term corresponding to the time derivative $\pi = \dot{\psi}$, for which we choose the standard ‘‘relativistic’’ form. The total energy is then given by

$$E_{\text{tot}} = \int d^2x \left[|\pi|^2 + \alpha|\psi|^2 + \frac{\beta}{2}|\psi|^4 + |\vec{D}\psi|^2 \right] + \frac{1}{2} \int d^3x (\mathbf{E}^2 + \mathbf{B}^2), \quad (4)$$

where we have used the covariant derivative $\vec{D}\psi = (\vec{\nabla} + ie\vec{A})\psi$. The full partition function is

$$Z = \int \mathcal{D}\psi \mathcal{D}\pi \mathcal{D}\mathbf{A} \mathcal{D}\mathbf{E} e^{-E_{\text{tot}}/T}. \quad (5)$$

This partition function describes the thermal equilibrium state of the system. We shall use the thermal ensemble as the ensemble of initial conditions for the time evolution, choosing a high enough temperature so that the film is initially in the normal phase.

The equations of motion are obtained by using E_{tot} as the Hamiltonian and identifying π^* as the canonical momentum conjugate to ψ . This gives the equations

$$\begin{aligned} \ddot{\psi} - \vec{D}^2\psi + \alpha\psi + \beta|\psi|^2\psi &= 0, \\ \vec{\mathbf{A}} + \nabla \times \nabla \times \mathbf{A} &= \mathbf{j}, \end{aligned} \quad (6)$$

where \mathbf{j} is the electric current. The latter equation is, of course, equivalent to Maxwell’s equations. The current is confined on the plane $z = 0$, i.e., $\mathbf{j} = \delta(z)(\vec{j}_x, \vec{j}_y, 0)$, where the two-dimensional current is $\vec{j} = 2e\text{Im}\psi^*\vec{D}\psi$.

Because Eq. (5) describes a thermal equilibrium state, the system stays in equilibrium if it is evolved according to Eqs. (6). In order to cool the system, we modify the equations by adding a damping term to the equation for ψ ,

$$\ddot{\psi} - \vec{D}^2\psi + \alpha\psi + \beta|\psi|^2\psi = -\sigma\dot{\psi}. \quad (7)$$

In order not to violate Gauss’s law $\nabla \cdot \mathbf{E} = \rho$, we need to modify the equation for the vector potential \mathbf{A} as well, by adding an Ohmic contribution to the electric current,

$$\mathbf{j} = \delta(z)(\vec{j}_x, \vec{j}_y, 0) + \sigma\mathbf{E}, \quad (8)$$

where the damping rate σ plays the role of the conductivity.

When the system is evolved according to these equations, the total energy gradually decreases. Strictly speaking, the system will not be in thermal equilibrium, but using a suitable effective definition of temperature,

one can say that it cools down. If α is negative, the system will eventually reach the critical temperature at which the film becomes superconducting.

Note that Eq. (7), with an appropriate rescaling, becomes the usual time-dependent Ginzburg-Landau equation in the limit $\sigma \rightarrow \infty$. However, σ determines the rate of cooling of the system, which we want to be able to vary. Therefore, we have to keep the second-order terms both in Eq. (7) and in the Maxwell equation.

A damping term like this is not the only possible way to induce a phase transition. In Ref. 19, this was done by varying the quadratic term α at constant temperature. We do not believe the qualitative phenomena we are interested in are sensitive to the specific choice, but quantitative details may well be different.

III. FLUX TRAPPING

As long as the system is in the normal phase, it will stay close to thermal equilibrium, because the film does not affect the dynamics of the vector potential significantly. To a good approximation, the Fourier modes of the orthogonal magnetic field $B = \partial_x \vec{A}_y - \partial_y \vec{A}_x$ with wave number \vec{k} greater than σ will oscillate with a decreasing amplitude

$$B(\vec{k}) \sim \exp(-\sigma t/2) \cos(kt). \quad (9)$$

The equilibrium distribution given by Eq. (5) is approximately Gaussian in the normal phase, and it can therefore be completely characterized by the two-point function

$$\langle B(\vec{k})B(\vec{k}') \rangle \equiv G(|\vec{k}|)(2\pi)^2 \delta(\vec{k} + \vec{k}'), \quad (10)$$

where²⁷

$$G(k) \approx \frac{Tk}{2}. \quad (11)$$

Thus, the modes with $|\vec{k}| \ll \sigma$ retain the equilibrium distribution with an exponentially decreasing effective temperature $T_{\text{eff}}(t) \approx T_{\text{ini}} \exp(-\sigma t)$.

When the temperature reaches the critical value T_c , the order parameter ψ becomes non-zero and the dynamics becomes non-linear. If the system were to stay in equilibrium, it would now be in the superconducting phase and therefore repel magnetic fields.

The equilibrium two-point function is²⁷

$$G(k) \approx \frac{Tk}{2} \frac{1}{1 + k\Lambda}, \quad (12)$$

where Λ is a screening length that starts from zero at T_c and grows exponentially as the temperature decreases. At any finite temperature, thermal fluctuations with wavelength less than Λ are suppressed relative to the normal phase, but longer wavelengths are unaffected. This

means that there is no sharp transition but the apparent critical temperature depends on the length scale.

Even though it is impossible to solve the non-linear equations of motion analytically, we can generally say that the amplitude of a Fourier mode of B with wave number k cannot decay arbitrarily fast. Moreover, the longer wave lengths react slower. For instance, if the dynamics of the long-wavelength fluctuations is diffusive, the fastest possible decay rate is $\gamma_{\max}(k) = k^2/D$, where D is the diffusion constant. It is therefore unavoidable that if the transition takes place in a finite time, the longest wavelengths are too slow to react, and freeze out. This means that there is a critical wave number k_c so that modes with $k < k_c$ still have approximately their initial amplitude after the transition.

The survival of the long-wavelength fluctuations means that at distances less than $1/k_c$, there is effectively a uniform magnetic field. If this length scale is longer than the Pearl length, i.e., the size of a vortex, this magnetic field must form an Abrikosov vortex lattice.¹⁹ This mechanism of vortex formation is called flux trapping.

The number density of vortices per unit area produced by flux trapping is approximately²⁷

$$n \approx \frac{e}{2\pi} \sqrt{\frac{T_c k_c^3}{2\pi}}. \quad (13)$$

Moreover, because the frozen-out magnetic field consists of modes with wavelengths longer than $2\pi/k_c$, there are clusters of size $2\pi/k_c$ of equal-sign vortices. We can estimate the number of vortices in each cluster by assuming that they are disks of radius $1/k_c$.

$$N_{\text{cl}} \approx \sqrt{\frac{e^2 T_c}{8\pi k_c}} \quad (14)$$

vortices. For the estimate in Eq. (13) to be valid, N_{cl} has to be greater than one. Otherwise, one will have to consider the coupled dynamics of both the electromagnetic field and the order parameter. It seems likely that vortex formation can then be described by the Kibble-Zurek mechanism,^{16,17,18} although the electromagnetic field may still play a role.

In fact, the friction term σ causes modes with $|\vec{k}| \lesssim \sigma$ to freeze out even in the absence of any critical dynamics. The solution of the linearized equations of motion with thermal initial conditions gives

$$\begin{aligned} G(k) &= T e^{-\sigma t} \int \frac{dk_z}{2\pi} \frac{\vec{k}^2}{k^2} \left[\frac{\sigma^2}{\tilde{\sigma}^2} \cosh \tilde{\sigma} t + \frac{\sigma}{\tilde{\sigma}} \sinh \tilde{\sigma} t - \frac{4\mathbf{k}^2}{\tilde{\sigma}^2} \right] \\ &\approx T \int \frac{dk_z}{2\pi} \frac{\vec{k}^2}{k^2} e^{-(2k^2/\sigma)t} = \frac{Tk}{2} \text{Erfc} \sqrt{2k^2 t/\sigma}, \quad (15) \end{aligned}$$

where $\mathbf{k}^2 = \vec{k}^2 + k_z^2$ and $\tilde{\sigma}^2 = \sigma^2 - 4\mathbf{k}^2$, and Erfc is the complementary error integral. The second line is valid at late times when $|\vec{k}| \ll \sigma$. This gives rise to an apparent critical wave number $k_c = \sqrt{\sigma/2t}$.

We are mainly interested in the physically more relevant case in which the freeze-out is caused by the critical dynamics, which restricts us to relatively low damping rates σ . Nevertheless, simulations with higher σ are also useful, because we can make more precise theoretical predictions using the exact two-point function (15).

IV. FLUX QUANTIZATION

Let us now assume that at the freeze-out, the two-point function is given by some function $G(k)$, and calculate how many vortices should be formed. If the amplitude of the frozen-out fluctuations is high enough, this can be done by considering a circular region of radius R . We assume that the magnetic field is more or less uniform at this length scale and that the magnetic flux $\Phi(R)$ through this region is much greater than one flux quantum $2\pi/e$. In that case, the number of vortices $N(R)$ is given by the flux

$$N(R) = n\pi R^2 = \frac{e}{2\pi} |\Phi(R)| = \frac{e}{2\pi} \left| \int_0^R d^2x B(\vec{x}) \right|, \quad (16)$$

where n is the number density of vortices per unit area. We can therefore write

$$n^2 = \lim_{R \rightarrow 0} \frac{e^2}{4\pi^4 R^4} \langle \Phi(R)^2 \rangle. \quad (17)$$

It is straightforward to write $\langle \Phi(R)^2 \rangle$ in terms of $G(k)$,

$$\begin{aligned} \langle \Phi(R)^2 \rangle &= \int d^2x d^2y \langle B(\vec{x}) B(\vec{y}) \rangle \\ &= R^4 \int d^2k \left(\frac{J_1(kR)}{kR} \right)^2 G(k) \\ &\xrightarrow{R \rightarrow 0} \frac{R^4}{4} \int d^2k G(k), \quad (18) \end{aligned}$$

where $J_1(kR)$ is a Bessel function. Thus, we expect

$$n = \frac{e}{4\pi^2} \left(\int d^2k G(k) \right)^{1/2}. \quad (19)$$

In the friction-dominated case, we can combine the integrations in Eqs. (15) and (19) into one integral,

$$\begin{aligned} n^2 &= \frac{e^2 T e^{-\sigma t}}{12\pi^4} \int d\mathbf{k} \mathbf{k}^2 \left[\frac{\sigma^2}{\tilde{\sigma}^2} \cosh \tilde{\sigma} t + \frac{\sigma}{\tilde{\sigma}} \sinh \tilde{\sigma} t - \frac{4\mathbf{k}^2}{\tilde{\sigma}^2} \right] \\ &\approx \frac{e^2 T}{12\pi^4} \int d\mathbf{k} \mathbf{k}^2 e^{-2\mathbf{k}^2 t/\sigma} = \frac{e^2 T}{48\pi^2} \left(\frac{\sigma}{2\pi t} \right)^{3/2}, \quad (20) \end{aligned}$$

where the approximate equality is valid at late times. In principle, t should be chosen to be the time the vortices form.

For slower σ , the two-point function $G(k)$ cannot be calculated analytically, but we assume that it can still be approximated by a Gaussian function,

$$G(k) = \frac{T_2 k}{2} e^{-(k/k_2)^2}, \quad (21)$$

where T_2 and k_2 are constants. Then, Eq. (19) yields

$$n^2 = \frac{e^2 T_2 k_2^3}{64\pi^{5/2}}. \quad (22)$$

The number of vortices per cluster is roughly given by $N_{\text{cl}} \approx n\pi/k_c^2$, which gives

$$N_{\text{cl}} \approx \sqrt{\frac{e^2 T_2}{64\pi^{1/2} k_2}}, \quad (23)$$

and in principle this number should be much greater than one for Eq. (16), and consequently also these estimates, to be valid.

It is important to note that Eqs. (15) and (21) are idealized descriptions of what the two-point function $G(k)$ should look like at the time of the freeze-out, when the magnetic field is still smooth over long distances. When the vortices form, the magnetic flux is quantized and this introduces microscopic structure to the two-point function. This will be important when we measure it and attempt to extract the fit parameters.

Let us first assume that N vortices and N antivortices are formed, and that they are point-like so that their magnetic field can be described by a sum of delta functions,

$$B(\vec{x}) = \frac{2\pi}{e} \sum_{i=1}^N [\delta(x - x_i^+) - \delta(x - x_i^-)], \quad (24)$$

where \vec{x}_i^\pm are the positions of the vortices and antivortices. The two-point function is

$$\langle B(\vec{x})B(\vec{y}) \rangle = \frac{4\pi^2}{e^2} \sum_{ij} G_{ij}(\vec{x} - \vec{y}), \quad (25)$$

where the two-vortex correlator $G_{ij}(\vec{x} - \vec{y})$ is

$$G_{ij}(\vec{x} - \vec{y}) = \langle [\delta(\vec{x} - \vec{x}_i^+) - \delta(\vec{x} - \vec{x}_i^-)] [\delta(\vec{y} - \vec{x}_j^+) - \delta(\vec{y} - \vec{x}_j^-)] \rangle, \quad (26)$$

and the brackets $\langle \rangle$ indicate integration over the positions \vec{x}_i^\pm .

As long as $i \neq j$, $G_{ij}(\vec{x} - \vec{y}) = G_0(\vec{x} - \vec{y})$ is independent of i and j . On the other hand, for $i = j$, we have

$$\begin{aligned} G_{ii}(\vec{x} - \vec{y}) &= \langle \delta(\vec{x} - \vec{x}_i^+) \delta(\vec{y} - \vec{x}_i^+) \rangle \\ &+ \langle \delta(\vec{x} - \vec{x}_i^-) \delta(\vec{y} - \vec{x}_i^-) \rangle \\ &- \langle \delta(\vec{x} - \vec{x}_i^+) \delta(\vec{y} - \vec{x}_i^-) \rangle \\ &- \langle \delta(\vec{x} - \vec{x}_i^-) \delta(\vec{y} - \vec{x}_i^+) \rangle. \end{aligned} \quad (27)$$

The two last terms give contributions of order N/A^2 , which we will ignore but the two first give delta functions, so

$$G_{ii}(\vec{x} - \vec{y}) = 2\delta(\vec{x} - \vec{y})/A, \quad (28)$$

where A is the area of the film.

electric charge	e	0.3
coupling constants	α	-0.25
	β	0.18
lattice size	N^3	512^3
lattice spacing	δx	1.0
time step	δt	0.05
initial temperature	T_{ini}	10.0
thermalization cycles	N_{th}	16
time evolved in each	t_{th}	32.0

TABLE I: Parameter values

In total, we have in Fourier space,

$$G(k) = \frac{4\pi^2}{e^2} [(2N/A) + N(N-1)G_0(k)]. \quad (29)$$

The continuous-field limit is basically equivalent to taking $N \rightarrow \infty$, and $2N/A = n$ is the number density of vortices, so we find

$$G(k) = \frac{4\pi^2 n}{e^2} + G_{\text{cont}}(k), \quad (30)$$

where $G_{\text{cont}}(k)$ is the two-point function given by the continuous magnetic field.

Of course, the magnetic field is not completely localized, which means that the delta functions spread over a finite distance. If we write the Fourier transform of the magnetic field profile of a vortex as $G_1(k)$, we have

$$G(k) = \frac{4\pi^2 n}{e^2} G_1(k) + G_{\text{cont}}(k). \quad (31)$$

We use the Gaussian ansatz in Eq. (21) for $G_{\text{cont}}(k)$. In principle, $G_1(k)$ could be calculated by finding the static vortex solution, but we simply parameterize it by an exponential, so that the whole two-point function is

$$G(k) = \frac{T_1 k}{2} e^{-k/k_1} + \frac{T_2 k}{2} e^{-(k/k_2)^2}. \quad (32)$$

We will use this form for fitting our numerical results. The above discussion predicts that k_1 should not depend on the nature of the quench, because it is a property of the static solution. The value of T_1 should be proportional to the number of vortices.

The linearized result in Eq. (15) is not of exactly the same form as Eq. (21), and therefore the parameters T_2 and k_2 will not be exactly the same as their theoretical values in the fast-quench limit, but they should still be close to them.

V. SIMULATIONS

We tested our predictions by solving the fully non-linear equations of motion (A5) numerically using the initial conditions given by the partition function (5). To

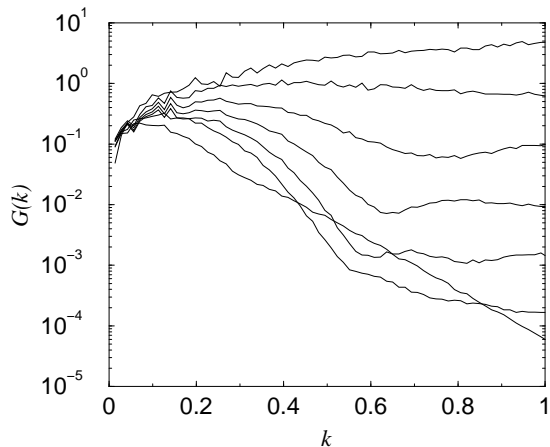


FIG. 1: Time evolution of the two-point function at $\sigma = 1.0$. From top to bottom, the curves correspond to $t = 0, 2, 4, 6, 8, 10$ and 20 .

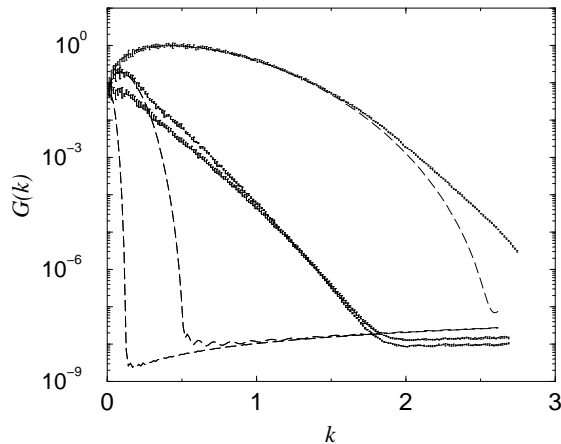


FIG. 2: The measured two point function $G(k)$, and the linearized prediction calculated numerically from Eq. (15) [dashed lines]. From left to right, the curve pairs correspond to $\sigma = 0.25, \sigma = 1.0$ and $\sigma = 5.0$.

do this, we defined the system on a three-dimensional lattice, one slice of which corresponds to the film. The details of the lattice implementation are presented in Appendix A.

In the preparation of the thermal initial conditions we employed the fact that the energy functional E_{tot} in Eq. (A7) is quadratic and diagonal in \mathbf{E} and π . Therefore, their probability distribution is Gaussian. The only complication is the Gauss law (A6), without which the field values at different points would be uncorrelated.

To generate the initial conditions, we first drew random, uncorrelated values for the component of π that is parallel to ψ , i.e., $\pi_\psi = \psi(\text{Re}\psi^*\pi)/(\psi^*\psi)$. This component does not appear in the Gauss law (A6), and therefore it has the simple Gaussian probability distribution

$$p[\pi_{\psi,(\bar{x})}] \propto \exp\left[-\frac{\delta x^2}{T}\pi_{\psi,(\bar{x})}^2\right]. \quad (33)$$

Then, we went through all plaquettes and considered a change of the electric field at all links around the plaquette by the same amount,

$$\begin{aligned} \mathbf{E}_{i,(\mathbf{x})} &\rightarrow \mathbf{E}_{i,(\mathbf{x})} + \epsilon, \\ \mathbf{E}_{j,(\mathbf{x})+\hat{i}} &\rightarrow \mathbf{E}_{j,(\mathbf{x})+\hat{i}} + \epsilon, \\ \mathbf{E}_{i,(\mathbf{x})+\hat{j}} &\rightarrow \mathbf{E}_{i,(\mathbf{x})+\hat{j}} - \epsilon, \\ \mathbf{E}_{j,(\mathbf{x})} &\rightarrow \mathbf{E}_{j,(\mathbf{x})} - \epsilon. \end{aligned} \quad (34)$$

Such a change does not change the divergence of \mathbf{E} and therefore does not affect the Gauss law constraint. It would change the energy by an amount that is at most quadratic in ϵ ,

$$\Delta E_{\text{tot}}(\epsilon) = Q\epsilon^2 + L\epsilon, \quad (35)$$

where the constants Q and L depend on the field values at the neighbouring links. Therefore the probability distribution for ϵ is Gaussian,

$$p[\epsilon] \propto \exp\left[-\frac{\Delta E_{\text{tot}}(\epsilon)}{T}\right]. \quad (36)$$

It is straightforward to draw the value of ϵ from this distribution.

Next we evolved the field configuration for time t_{th} using the equations of motion (A5), with zero conductivity. We repeated this cycle of randomization and evolution steps N_{th} times, monitoring the evolution of the two-point function $G(k)$. When it reached the equilibrium form given by the analytical calculation, we considered the system to have thermalized.

We then solved the equations of motion (A5) with the initial conditions produced by the thermalization algorithm. We used a number of different values for the conductivity σ to test the dependence on the cooling rate, and for each value we repeated the run several times using different initial conditions from the same ensemble. The values of the other parameters are shown in Table I.

VI. RESULTS

Our main aim was to test the flux trapping theory, and therefore we measured the two-point function $G(k)$ of the magnetic field fluctuations on the film. In Fig. 1, we show the time evolution of $G(k)$ for $\sigma = 1.0$. One can see that, as expected, the long-wavelength modes freeze out to a high amplitude, whereas short wavelengths are exponentially suppressed. The plot also shows how the amplitude at around $0.3 \lesssim k \lesssim 0.8$ increases after $t \approx 10$, when the system enters the superconducting phase and the two-point function changes from Eq. (21) to Eq. (32) because of flux quantization.

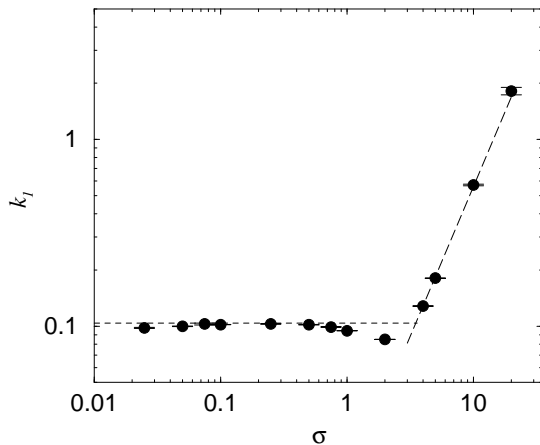


FIG. 3: The exponential cutoff scale k_1 as a function of σ . For $\sigma \rightarrow 0$ it approaches a constant value $k_1 = 0.104(1)$, which characterizes the size of a static isolated vortex solution. At high σ , vortex density is high and the system still away from equilibrium, and the vortices are not well described by the static solution. In this regime, we fit $k_1 = 0.0140(6)\sigma^{1.60(3)}$. In all other fits, we fixed $k_1 = 0.1$.

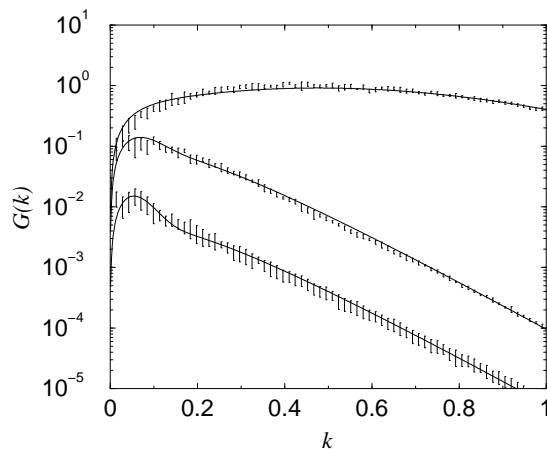


FIG. 4: Two point functions $G(k)$ together with fits of the form (32). From top to bottom, the curves correspond to $\sigma = 5.0, 0.5$ and 0.05 .

To make it possible to compare the results for different values of σ , we chose to carry out our measurements at time $t = 20/\sigma$, so that the effective temperature is the same in each case. Fig. 2 shows the measured two-points function at that time for selected values of σ . They are compared with the results for linearized friction-dominated freeze-out, calculated numerically from the first line of Eq. (15). The plot shows that the linearized result works very well in fast quenches. For $\sigma \lesssim 1$, one can see a clear discrepancy, which is a sign that the non-linear effects have become important. The difference is also partly due to the contribution $G_1(k)$ from flux quantization.

We fitted the two-point functions with the ansatz in

Eq. (32). In Fig. 3, we show k_1 as a function of σ . As expected, its value is independent of σ in slow quenches. At higher σ , the vortex density becomes higher and non-equilibrium effects more important, and therefore it is not surprising that k_1 starts to grow. This can be interpreted as the size of the vortex getting smaller as more of them are packed in the same area.

To improve the accuracy of the fit parameters in subsequent fits, we fixed k_1 to 0.1. Some examples of these fits are shown in Fig. 4. The plateau at very short wavelengths, which corresponds to modes still in thermal equilibrium was excluded from the fits.

In Fig. 5 we show the fit parameters T_1 , T_2 and k_2 as functions of σ . The errors were estimated using the bootstrap method, and contain only the statistical error. We did not attempt to estimate the systematic error in any measurement due to the choice of the fitting function.

In the high- σ limit, the two-point function should be given by Eq. (15), and to the extent that it can be approximated by a Gaussian, we expect $T_2 \approx T = 10$ and $k_2 \approx \sqrt{\sigma/2t}$. This is confirmed by the measurements. In this limit the values of T_1 show significant scattering, but this understandable, because $G(k)$ is dominated by the Gaussian term and we had also fixed k_1 to a very different value from the best fit.

In the opposite limit of low cooling rates, the parameters seem to be well described by power laws,

$$\begin{aligned} T_1 &\sim 9.76(9)\sigma^{1.218(6)}, \\ T_2 &\sim 2.6(5)\sigma^{0.43(6)}, \\ k_2 &\sim 0.186(5)\sigma^{0.318(8)}. \end{aligned} \quad (37)$$

The deviation from the linear prediction $k_2 \approx \sqrt{\sigma/2t}$ is a sign of non-linear dynamics. It is interesting to note, but possibly a coincidence, that the behaviour of T_2 appears to agree with the same power law even at $\sigma \approx 10$.

Fig. 6 shows the number of vortices plus antivortices measured at time $\sigma t = 20$. The agreement with the analytical prediction Eq. (20) shown by the dashed line is good for fast quenches $\sigma \gtrsim 1$, apart from a constant factor of about 2. This indicates that vortices are predominantly formed by flux trapping.

For $\sigma \lesssim 1$, we can fit the data very well with a power law $N = 772(18)\sigma^{1.20(2)}$. This is compatible with the expectation that $T_1 \propto N$. We have also plotted the theoretical prediction in Eq. (22) calculated using the fitted parameter values. As the plot shows, it gives the correct order of magnitude, although it does not agree perfectly for slow quenches. The prediction seems to suggest a different power-law behaviour from the observed one.

As Fig. 1 shows, the fluctuations have frozen out, but it is possible that their amplitude is not high enough to actually dominate the process of vortex formation. Indeed, if one estimates the typical number of vortices in a cluster using Eq. (23) one finds it decreases rapidly at low σ (see Fig. 7). In principle, the flux trapping mechanism requires this number to be greater than one. This

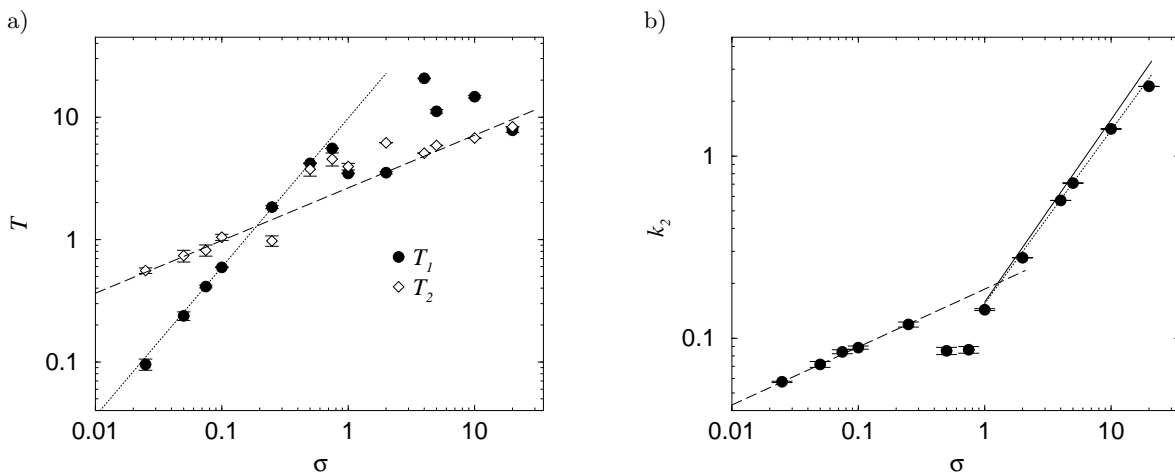


FIG. 5: Fit parameters T_1 , T_2 and k_2 as functions of σ . (a) Coefficients T_1 (filled circles) and T_2 (empty diamonds) of the exponential and Gaussian terms in Eq. (32) respectively. The dotted line shows the power-law fit $T_1 = 9.76(9)\sigma^{1.218(6)}$ to the first six data points. The dashed line shows a fit $T_2 = 2.6(5)\sigma^{0.43(6)}$ to the first four data points. (b) The critical wave-number k_2 . The solid line shows the theoretical prediction $k_2 = \sqrt{\sigma/2t}$, and the dashed and dotted lines are power-law fits $k_2 = 0.186(5)\sigma^{0.318(8)}$ and $k_2 = 0.115(7)\sigma^{0.95(3)}$ of the first five and last six data points, respectively.

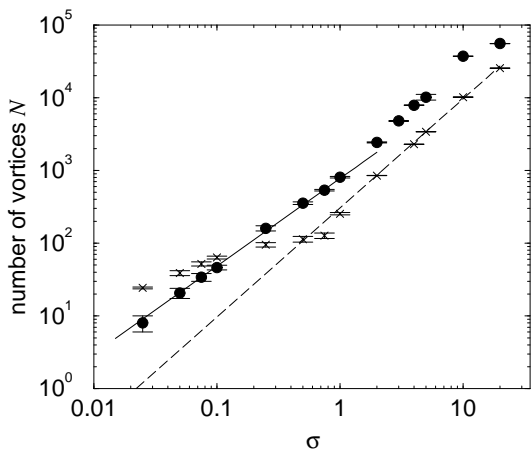


FIG. 6: Vortex number measured at $\sigma t = 20$ as a function of σ . The dashed line shows the theoretical prediction (20) for fast quenches, and the solid line a a power-law fit $N = 772(18)\sigma^{1.20(2)}$ of data at $\sigma \leq 0.5$. The crosses show the prediction (22) for slow quenches based on the fit parameters T_2 and k_2 .

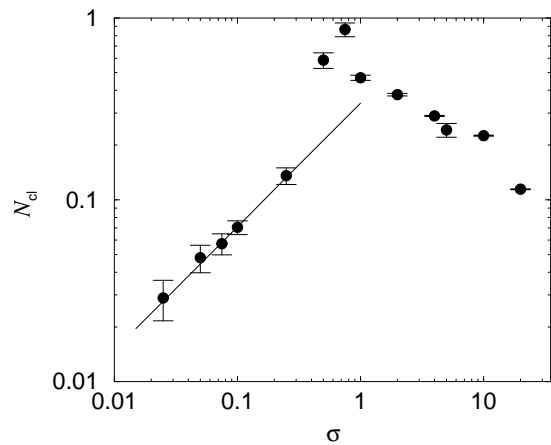


FIG. 7: The number of vortices in each cluster calculated from the measured vortex density and the fit parameter k_2 .

typical number of vortices in a cluster.

suggest that the slow quenches could possibly be better described by the Kibble-Zurek mechanism.

It is possible to increase N_{cl} by using different parameter values, and we carried out one set of runs with $T = 1000$. The clustering is indeed evident in the snapshot of the magnetic field at time $t = 400$ in a run with $\sigma = 0.25$ shown in Fig. 8. In the same figure, we have also plotted the quantity, $n_C(r)$ which measures the average winding number around a circle of radius r centered at a vortex.¹⁹ Clustering is indicated by values greater than one, and the maximum value gives a measure of the

VII. CONCLUSIONS

In fast quenches $\sigma \gg 1$, the two-point function $G(k)$ of the magnetic field fluctuations is consistent with the predictions of the linearized theory. This allows us to calculate the number of vortices produced by flux trapping, and this prediction agrees very well with the measured values. This provides strong support for the flux trapping scenario of vortex formation. Furthermore, the spatial distribution of vortices shows the tell-tale signal of vortex clusters.

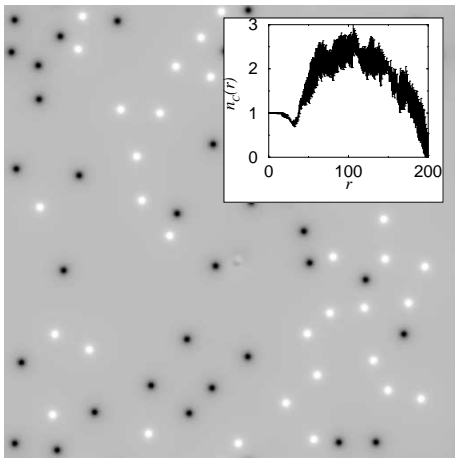


FIG. 8: The magnetic field configuration on the film at time $t = 400$ in a run with $T = 1000$ and $\sigma = 0.25$. The curve in the inset shows the quantity $n_C(r)$, which measures clustering.

It should be kept in mind that in fast quenches, the relevant degrees of freedom are overdamped. This is not necessarily a problem, because it can be given a physical interpretation as a relatively high conductivity. Furthermore, overdamped dynamics is commonly used in studies of superconductors and vortex formation.²⁸ Nevertheless, for many applications underdamped dynamics would probably be better. Ideally one should carry out the simulation without introducing damping at all,^{19,29} but even in our case, the relevant degrees of freedom are underdamped in slow quenches.

The underdamped nature of dynamics makes it much more difficult to describe slow quenches theoretically, and therefore the predictions are not as robust. In spite of this, our results show a reasonably good agreement between theory and simulation, although the scaling of the vortex number with the cooling rate σ does not seem to agree. This may be an indication that the amplitude of trapped fluctuations is so low that vortex formation can be better described by the Kibble-Zurek mechanism.

Simulations with a higher initial temperature support this picture, and show clear vortex clustering even in slow quenches. This is an unmistakable sign of flux trapping

To understand better how vortices form when the amplitude is not high enough for flux trapping, it would be important to derive theoretical predictions of the Kibble-Zurek scenario and compare them with our results. In particular, one must understand how a weak background magnetic field biases the Kibble-Zurek mechanism.

Our results show that under the right conditions, the electromagnetic field plays an important role in defect formation. It remains to be seen if these conditions are satisfied in actual superconductor experiments. Likewise, the cosmological consequences of this remain largely unexplored.

Acknowledgments

This work was supported by Churchill College, Cambridge (A.R.), Cambridge European Trust and EPSRC (M.D.). We also acknowledge support from the European Science Foundation, through the COSLAB (Cosmology in the Laboratory) programme. This research was conducted in cooperation with SGI/Intel utilising the Altix 3700 supercomputer.

APPENDIX A: LATTICE DISCRETIZATION

To write down the discretized equation of motion, we define the forward and backward derivatives

$$\Delta_i^\pm f(\mathbf{x}) = \pm \delta x^{-1} (f(\mathbf{x} \pm \hat{i}) - f(\mathbf{x})), \quad (\text{A1})$$

where δx is the lattice spacing and \hat{i} is a unit vector in the i direction. Similarly, we define the time derivative

$$\Delta_t f(t) = \delta t^{-1} (f(t) - f(t - \delta t)), \quad (\text{A2})$$

where δt is the time step. Using the link variable

$$\vec{U}_i = \exp(i e \delta x \vec{A}_i), \quad (\text{A3})$$

we also define the corresponding covariant derivatives on the film

$$\begin{aligned} \vec{D}_i^+ \psi(\vec{x}) &= \delta x^{-1} (\vec{U}_{i,(\vec{x})} \psi(\vec{x} + \hat{i}) - \psi(\vec{x})), \\ \vec{D}_i^- \psi(\vec{x}) &= \delta x^{-1} (\psi(\vec{x}) - \vec{U}_{i,(\vec{x} - \hat{i})}^* \psi(\vec{x} - \hat{i})). \end{aligned} \quad (\text{A4})$$

The discretized equations of motion are

$$\begin{aligned} \Delta_t \mathbf{A}_{i,(t,\mathbf{x})} &= -\mathbf{E}_{i,(t-\delta t,\mathbf{x})}, \\ \Delta_t \psi(t,\vec{x}) &= \pi(t-\delta t,\vec{x}), \\ \Delta_t \mathbf{E}_{i,(t,\mathbf{x})} &= \sum_{jklm} \epsilon_{ijk} \epsilon_{klm} \Delta_j^- \Delta_l^+ \mathbf{A}_{m,(t,\mathbf{x})} - \sigma \mathbf{E}_{i,(t,\mathbf{x})} \\ &\quad - \frac{2e}{\delta x} \delta_z \text{Im} \psi_{(t,\vec{x})}^* \vec{D}_i^+ \psi(t,\vec{x}), \\ \Delta_t \pi(t,\vec{x}) &= \sum_i \vec{D}_i^- \vec{D}_i^+ \psi(t,\vec{x}) - \sigma \pi(t,\vec{x}) \\ &\quad - \alpha \psi(t,\vec{x}) - \beta |\psi(t,\vec{x})|^2 \psi(t,\vec{x}), \end{aligned} \quad (\text{A5})$$

where the summation over directions goes from 1 to either 2 or 3 depending on the context.

The lattice version of the Gauss law is

$$\sum_i \Delta_i^- \mathbf{E}_{i,(t,\mathbf{x})} = \frac{2e}{\delta x} \delta_z \text{Im} \psi_{(t,\vec{x})}^* \pi(t,\vec{x}). \quad (\text{A6})$$

This equality is exactly conserved by the lattice equations of motion and is a constraint the initial field configuration must satisfy.

The lattice version of the energy functional (4) is

$$\begin{aligned}
E_{\text{tot}} = & \frac{1}{2} \sum_{\mathbf{x}, i} \delta x^3 \left[\mathbf{E}_i^2 + \sum_{jk} (\epsilon_{ijk} \Delta_j^\dagger \mathbf{A}_k)^2 \right] \\
& + \sum_{\vec{x}} \delta x^2 \left[\pi^* \pi - \frac{2}{\delta x^2} \sum_i \text{Re} \psi_{(\vec{x})}^* \vec{U}_{i,(\vec{x})} \psi_{(\vec{x}+\hat{i})} \right. \\
& \left. + \left(\alpha + \frac{4}{\delta x^2} \right) |\psi|^2 + \frac{\beta}{2} |\psi|^4 \right]. \quad (\text{A7})
\end{aligned}$$

It should be noted that both the equations of motion (A5) and the energy functional (A7) are gauge invariant. In this non-compact lattice formulation, the gauge group is, in fact, \mathbb{R} rather than $U(1)$, which has the advantage that vortices are topologically stable even on lattice.

In the actual simulations, we used a finite lattice with periodic boundary conditions in all three directions. This has the consequence that the net magnetic flux through the film vanishes.

-
- ¹ R. Carmi and E. Polturak, Phys. Rev. B **60**, 7595 (1999).
² R. Carmi, E. Polturak, and G. Koren, Phys. Rev. Lett. **84**, 4966 (2000).
³ E. Kavoussanaki, R. Monaco, and R. J. Rivers, Phys. Rev. Lett. **85**, 3452 (2000), cond-mat/0005145.
⁴ R. Monaco, J. Mygind, and R. J. Rivers, Phys. Rev. Lett. **89**, 080603 (2002).
⁵ R. Monaco, J. Mygind, and R. J. Rivers, Phys. Rev. B **67**, 104506 (2003).
⁶ J. R. Kirtley, C. C. Tsuei, and F. Tafuri, Phys. Rev. Lett. **90**, 257001 (2003).
⁷ A. Maniv, E. Polturak, and G. Koren, Phys. Rev. Lett. **91**, 197001 (2003).
⁸ J. R. Kirtley, C. C. Tsuei, F. Tafuri, P. G. Medaglia, P. Orgiani, and G. Balestrino, Supercond. Sci. Technol. **17**, S217 (2004).
⁹ C. Bauerle et al., Nature **382**, 332 (1996).
¹⁰ V. M. H. Ruutu et al., Nature **382**, 334 (1996), cond-mat/9512117.
¹¹ M. E. Dodd, P. C. Hendry, N. S. Lawson, P. V. E. McClintock, and C. D. H. Williams, Phys. Rev. Lett. **81**, 3703 (1998).
¹² I. Chuang, R. Durrer, N. Turok, and B. Yurke, Science **251**, 1336 (1991).
¹³ M. J. Bowick, L. Chandar, E. A. Schiff, and A. M. Srivastava, Science **263**, 943 (1994), hep-ph/9208233.
¹⁴ S. Digal, R. Ray, and A. M. Srivastava, Phys. Rev. Lett. **83**, 5030 (1999), hep-ph/9805502.
¹⁵ R. Ray and A. M. Srivastava, Phys. Rev. **D69**, 103525 (2004), hep-ph/0110165.
¹⁶ T. W. B. Kibble, J. Phys. **A9**, 1387 (1976).
¹⁷ T. W. B. Kibble, Phys. Rept. **67**, 183 (1980).
¹⁸ W. H. Zurek, Phys. Rept. **276**, 177 (1996), cond-mat/9607135.
¹⁹ M. Hindmarsh and A. Rajantie, Phys. Rev. Lett. **85**, 4660 (2000), cond-mat/0007361.
²⁰ A. Rajantie, Int. J. Mod. Phys. **A17**, 1 (2002), hep-ph/0108159.
²¹ A. Vilenkin and E. Shellard, *Cosmic strings and other topological defects* (Cambridge University Press, 1994).
²² G. Dvali and A. Vilenkin, JCAP **0403**, 010 (2004), hep-th/0312007.
²³ M. Sazhin et al., Mon. Not. Roy. Astron. Soc. **343**, 353 (2003), astro-ph/0302547.
²⁴ R. E. Schild, I. S. Masnyak, B. I. Hnatyk, and V. I. Zhdanov (2004), astro-ph/0406434.
²⁵ M. V. Sazhin et al. (2004), astro-ph/0406516.
²⁶ H. B. Nielsen and P. Olesen, Nucl. Phys. **B61**, 45 (1973).
²⁷ T. W. B. Kibble and A. Rajantie, Phys. Rev. **B68**, 174512 (2003), cond-mat/0306633.
²⁸ G. J. Stephens, L. M. A. Bettencourt, and W. H. Zurek, Phys. Rev. Lett. **88**, 137004 (2002), cond-mat/0108127.
²⁹ M. Hindmarsh and A. Rajantie, Phys. Rev. **D64**, 065016 (2001), hep-ph/0103311.